FULL PAPER

Plasmonic Janus-Composite Photocatalyst Comprising Au and C–TiO_2 for Enhanced Aerobic Oxidation over a Broad Visible-Light Range

*Lequan Liu, Thang Duy Dao, Rajesh Kodiyath, Qing Kang, Hideki Abe, Tadaaki Nagao, and Jinhua Ye**

Asymmetric Janus nanostructures containing a gold nanocage (NC) and a carbon–titania hybrid nanocrystal (AuNC/(C–TiO_2)) are prepared using a novel and facile microemulsion-based approach that involves the assistance of ethanol. The localized surface plasmon resonance of the Au NC with a hollow interior and porous walls induce broadband visible-light harvesting in the Janus AuNC/(C–TiO_2). An acetone evolution rate of 6.3 μmol h^{-1} g^{-1} is obtained when the Janus nanostructure is used for the photocatalytic aerobic oxidation of *iso*-propanol under visible light (λ = 480–910 nm); the rate is 3.2 times the value of that obtained with C–TiO_2, and in photo-electrochemical investigations an approximately fivefold enhancement is obtained. Moreover, when compared with the core–shell structure (AuNC@(C–TiO_2) and a gold–carbon–titania system where Au sphere nanoparticles act as light-harvesting antenna, Janus AuNC/(C–TiO_2) exhibit superior plasmonic enhancement. Electromagnetic field simulation and electron paramagnetic resonance results suggest that the plasmon–photon coupling effect is dramatically amplified at the interface between the Au NC and C–TiO_2, leading to enhanced generation of energetic hot electrons for photocatalysis.

1. Introduction

Harvesting energy directly from sunlight is a very attractive and desirable way to solve environmental remediation and solar-energy conversion issues, in which photocatalysis has been proven to be one of the most promising methods.[1] Photocatalysis is a green technology because it is an ambient-temperature process that can completely decompose organic pollutants even at low levels.[2,3] Since the pioneering work of Fujishima and Honda in the 1970s,[4] TiO_2 has become the most extensively studied semiconductor in applications such as environmental cleaning and hydrogen energy production.[5] However, TiO_2 possesses a wide bandgap (≈3.2 eV for anatase TiO_2), which limits its photo-absorption to the UV region, accounting for ≈4% of total sunlight. Many strategies have been proposed to extend the TiO_2 absorption edges to the visible region, e.g., metal and nonmetal doping.[6,7] Recently, visible—and even near-infrared—light responses have been achieved over hybrids of TiO_2 and carbon (C–TiO_2); this offers an attractive method for overcoming the photo-absorption limitation of TiO_2.[8,9] Nevertheless, due to low efficiencies in the conversion of incident photons to chemically useful charge carriers on the surface, photochemical processes over C–TiO_2 often exhibit low rates. Attempts to solve this problem have mainly centered on the development of various carbon sources.[10–13] Much effort, from the perspective of both chemistry and practical applications, is required to address this issue not only through the optimization of the hybridization process but also through the development of new strategies.

Dr. L. Q. Liu, T. D. Dao, Dr. Q. Kang,
Dr. T. Nagao, Prof. J. H. Ye
International Center for Materials
Nanoarchitectonics (WPI-MANA)
National Institute for Materials Science (NIMS), 1–1 Namiki
Tsukuba, Ibaraki 305–0044, Japan
E-mail: jinhua.ye@nims.go.jp
T. D. Dao, Dr. T. Nagao
CREST, Japan Science and Technology Agency
4–1–8 Honcho, Kawaguchi, Saitama 332–0012, Japan
T. D. Dao, Dr. T. Nagao
Graduate School of Materials Science
Nara Institute of Science and Technology, Japan
Dr. R. Kodiyath, Dr. H. Abe, Prof. J. H. Ye
Environmental Remediation Materials Unit
National Institute for Materials Science (NIMS)
1–1 Namiki, Tsukuba, Ibaraki 305–0044, Japan
Dr. H. Abe, Prof. J. H. Ye
TU-NIMS Joint Research Center
School of Material Science and Engineering
Tianjin University
92 Weijin Road, Tianjin, P.R. China

DOI: 10.1002/adfm.201402088

Incorporating plasmonic nanoparticles of the coinage metals (Au, Ag, Cu NPs) has recently emerged as a promising new strategy for enhancing photocatalytic efficiency, known as localized surface plasmon resonance (LSPR) enhancement.[14,15] In pursuit of plasmonic enhancement for a wide range in the visible-light region, 2D Au and Ag nanostructures involving semiconductor composites have been studied.[16–19] We also demonstrated that broadband visible-light harvesting over TiO_2 can be achieved by introducing Au nanorods as antennas.[20] From the perspective of maximizing the LSPR intensity however, nanostructures with sharp edges or apexes dominated by local electromagnetic "hot spots" are more favorable.[21] The fascinating plasmon–photon coupling properties of the Au nanocage (NC) with a hollow interior and porous walls make it an excellent candidate; it already finds application in a number of technological areas including surface-enhanced Raman scattering and biomedical therapy.[22,23] To the best of our knowledge, few efforts have been made to utilize the plasmon–photon coupling effect of Au NCs for efficient plasmonic photocatalysis.

More importantly, plasmonic nanostructures that are designed for amplifying hot-spot generation are critical. It has been found that plasmonic enhancement is strongly dependent on the material composition and interface engineering.[24,25] For example, the non-centrosymmetric coupling of metal and semiconductor nanoparticles at small, interconnecting junctions has been reported to potentially generate extremely strong local electric nearfields through interparticle coupling.[26,27] Furthermore, taking into account the critical roles played by Au NPs (i.e., photon harvesting and electron or energy transfer), asymmetric Janus composite nanostructures are particularly attractive. Although a few attempts have been made to prepare Janus composite nanostructures,[24,28,29] a facile synthesis for asymmetric Janus composite nanostructures remains a great challenge.

In the present work, a novel and facile microemulsion-based approach involving the assistance of ethanol is developed for preparing an asymmetric Janus nanostructure comprising Au NC and the C–TiO_2 hybrid. A prominent plasmonic enhancement, in the broadband visible-light region, is achieved in both the photocatalytic aerobic oxidation of *iso*-propanol (IPA) and its photo-electrocatalytic evaluation over the Janus composite of Au NC and C–TiO_2 (labeled as AuNC/(C–TiO_2)). Moreover, compared with the AuNC@(C–TiO_2) core–shell structure or the system where spherical Au nanoparticles are light-harvesting antenna for C–TiO_2, Janus AuNC/(C–TiO_2) exhibited superior plasmonic enhancement. Plasmonic coupling and electron transfer in Janus AuNC/(C–TiO_2) were investigated with electromagnetic field simulation and electron paramagnetic resonance (EPR), respectively. These results indicate that the plasmon–photon coupling effect was dramatically amplified at the interface of the Au NC and the C–TiO_2 particle, which results in the enhanced generation of energetic hot electrons for photocatalysis.

2. Results and Discussion

A bright yellow sample of Ag nanocubes with an LSPR absorption located at 425 nm was obtained (**Figure 1**). Characteristic

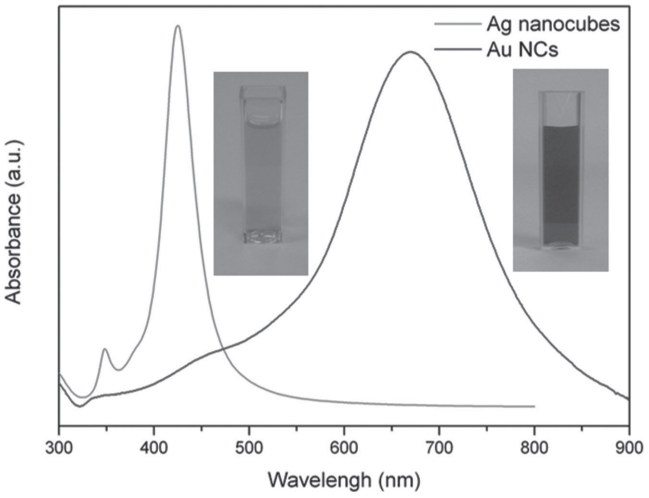

Figure 1. UV–vis absorption spectra of Ag nanocubes and Au NCs; insets: photographs of the yellow Ag nanocube and blue Au NC sample solutions.

multipolar excitations of the Ag nanocube at 380 and 350 nm were also observed in its optical-extinction spectrum, indicating that these particles were primarily cubic. Au NCs were prepared by reacting the as-prepared Ag nanocubes with $HAuCl_4$ in an aqueous medium. With increasing amounts of $HAuCl_4$, numerous pores within the walls of the Ag nanocube formed by the selective extraction of silver atoms, and porous Au NCs were then obtained. A blue sample of Au NCs with an LSPR absorption located at 675 nm was obtained (Figure 1). The morphology and nanostructure of the Ag nanocubes and Au NCs were further investigated using transmission electron microscopy (TEM). Ag nanocubes with an average edge length of 35 nm can be easily discerned in the TEM images (**Figure 2**a and in the Supporting Information (SI), Figure S1). As for the Au NCs, the skeleton was maintained during the replacement reaction between Ag and $HAuCl_4$, and pores on the cavity walls can be discerned (Figure 2b; Figure S2a,b, SI). A lattice space measured as 0.204 nm, corresponding to the Au(200) lattice plane, was observed in the high-resolution TEM image. Meanwhile, no obvious poly(vinyl pyrrolidone) (PVP) surfactant around the Au NC was observed because the replacement reaction was carried out after the Ag nanocubes were washed with ultrapure water (Figure S2c,SI).

A novel and facile microemulsion-based approach involving ethanol was developed for preparing the asymmetric Janus nanostructure comprising the Au NC and C–TiO_2 particle (**Figure 3**). An organic cyclohexane phase containing pre-synthesized, well-dispersed C–TiO_2 nanocrystals; an aqueous solution containing the Au NCs; and sodium dodecylsulfate (SDS) as surfactant were mixed together. A stable oil-in-water (O/W) microemulsion system was obtained by means of vigorous stirring, while the C–TiO_2 nanocrystals and Au NCs were dispersed in the oil and water phases, respectively. Surfactant is crucial for the formation of a microemulsion because it significantly reduces the surface tension of water, and the surface tension becomes roughly constant as further increase of the surfactant concentration. Co-surfactants (usually an alcohol with a C4–C6 aliphatic chain) have been found to be effective in further

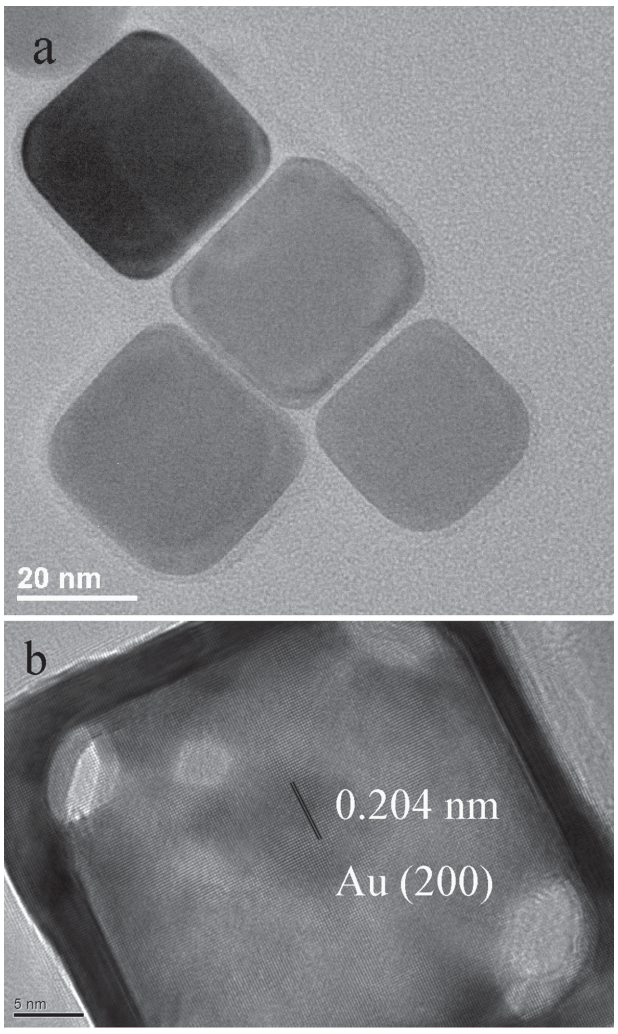

Figure 2. TEM images of a) Ag nanocubes and b) a Au NC.

decreasing the surface tension.[30] In this work, an appropriate amount of ethanol was added after the microemulsion formed, in order to partly introduce the Au NCs into the microemulsion oil droplets, where the C–TiO_2 nanocrystals are assembled. Ethanol with its polar functional group and short aliphatic tail served as a "co-surfactant" to a certain extent—from the fact that it further reduced the surface tension; however, it was introduced after microemulsion formation. Moreover, as suggested by De Gennes et al.,[31] ethanol can make the interface between oil and water flexible, which should be helpful for the migration of the Au NCs from water to microemulsion. Following the evaporation of the cyclohexane solvent, the composites of the Au NCs and C–TiO_2 were obtained. As can be seen from the TEM images (**Figure 4**a,b; Figure S3, SI), the Au NCs adhered to or were partly incorporated into the C–TiO_2 spheres with a diameter in the range of 60–80 nm; that is, the Janus AuNC/(C–TiO_2) nanostructure was successfully prepared with this ethanol-assisted microemulsion approach. Further increasing the amount of ethanol (to 1.0 mL) led to the Au NCs becoming surrounded by C–TiO_2, resulting in the AuNC@(C–TiO_2) core–shell structure (Figure 4c). This was expected because the surface tension becomes even lower as the amount of ethanol increases, which may result in the two phases becoming nearly identical and the interfacial region becoming very thick.[32] The diameter of the C–TiO_2 spheres increased to about 200 nm during this process, as verified by TEM, which should be caused by the aggregation of the C–TiO_2 spheres. For comparison, the system in which ≈20-nm Au NPs decorate a C–TiO_2 particle (AuNP/(C–TiO_2)) was prepared using a similar method (Figure 4d).

UV–vis absorption spectra of commercial anatase TiO_2 (from Wako, denoted as TiO_2-Commercial) and C–TiO_2 are shown in **Figure 5**a, while Tauc plots—$(\alpha h\nu)^{1/2}$ versus the energy of absorbed light—are provided in its inset; α, h, and ν represent the absorption coefficient of the material, Planck's constant, and frequency, respectively. As compared with TiO_2-Commercial, the overall visible-light absorbance intensities for C–TiO_2 was enhanced, and the absorption edge was red-shifted from 3.2 to 2.9 eV. The increased absorbance intensity was likely caused by the carbon centers on the surface of the TiO_2, which are known to act as a photosensitizer as a result of the coupling of the graphite-like carbon and the conduction-band states of TiO_2.[9] The red-shift of the absorption edge indicates that a small part of elemental carbon was doped into the TiO_2 lattice of the C–TiO_2.[33] Introducing Au NPs onto C–TiO_2 particles induce an LSPR absorption at 540 nm (Figure 5b), which is consistent with an earlier report.[34] An LSPR absorption centered at 700 nm covering broadband visible-light was obtained for Janus AuNC/(C–TiO_2), while a slight red-shift of the LSPR absorption to 710 nm for AuNC@(C–TiO_2) was likely caused by the change of host medium.[35]

Janus AuNC/(C–TiO_2) was further studied by Raman scattering. **Figure 6** shows the spectra of Janus AuNC/(C–TiO_2) and the analogous Janus system with commercial titania, Au NC/TiO_2-Commercial. A surface-enhanced Raman scattering (SERS) effect and characteristic peaks of anatase TiO_2 can be observed in both cases.[36] Nevertheless, Raman scattering bands due to carbon can be discerned in the spectra of Janus AuNC/(C–TiO_2) (inset image); more specifically, the peak at around 1586 cm^{-1} (G band) is associated with the E_{2g} vibrational mode of sp^2-hybridized carbon, i.e., a graphitic structure.[37] A hump at about 1350 cm^{-1} (D band), which is usually assigned to the vibrations of sp^3-hybridized carbon, can also be recognized. Meanwhile, the slope of above 1200 cm^{-1} in the spectrum of Janus AuNC/(C–TiO_2) indicates fluorescence interference which is likely caused by the resin polymers from dehydration of hydrocarbons. These results indicate: i) evidence of carbon is mainly for C–TiO_2; ii) the carbon observed

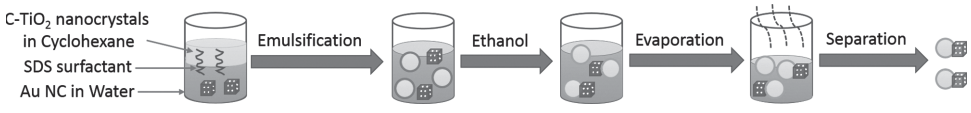

Figure 3. Schematic illustration of the preparation of Janus AuNC/(C–TiO_2).

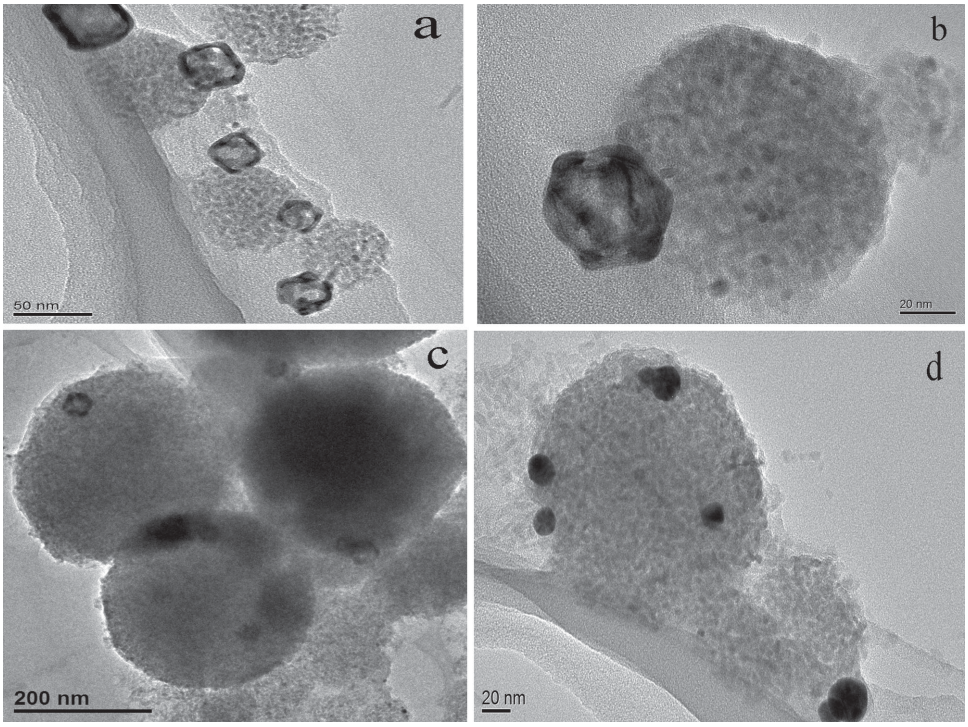

Figure 4. TEM images of a,b) Janus AuNC/(C–TiO_2) composites, c) AuNC@(C–TiO_2) core–shell particles, and d) AuNP/(C–TiO_2) composites.

in this Raman study are due to a mixture of sp^2- (graphite) and sp^3-hybridized carbon and the carbon of the resin polymers. Carbon is expected to originate from the triethylamine and the titanium alkoxide precursor itself from the preparation of the hybrid C–TiO_2 nanocrystals[13] (see Experimental Section). The carbon states in C–TiO_2 were investigated by X-ray photoelectron spectroscopy (XPS), and the binding energy of C 1s is available in the SI (Figure S4). Primary relevant C 1s peaks were found mainly at 284.5 and 288 eV. The first peak is ascribed to carbon with a C–C bond, which is attributed to the presence of hybridized carbon as well as organic impurities on the TiO_2 surface.[10] The binding energy at 288 eV is attributed to the presence of Ti–O–C units, as suggested in an earlier report;[38] that is, in addition to carbon on the surface of C–TiO_2, there is carbon doped into the lattice of TiO_2. Thermogravimetric/differential thermal analysis (TG/DTA) of Janus AuNC/(C–TiO_2) was also carried out (Figure S5, SI). There is an exothermic peak with a shoulder in the range of 150–450 °C accompanied with a continuous weight loss. The exothermic peak is attributed to the oxidation of carbon in C–TiO_2 to CO_2. During this process, the weight loss was about 27%.

X-ray diffraction patterns were also recorded for the as-prepared samples (Figure S6, SI). Characteristic anatase TiO_2 diffraction peaks can be easily discerned, suggesting high-quality crystallinity in C–TiO_2. Moreover, the Au(200), –(220), and –(311) diffraction planes with 2θ at 44.38°, 64.56°, and 77.55°, respectively, can be recognized for AuNC/(C–TiO_2), AuNP/(C–TiO_2), and AuNC@(C–TiO_2). N_2-adsorption measurements gave a specific surface area of 5.8 m^2 g^{-1} for Janus AuNC/(C–TiO_2) (Figure S7, SI). The gold loadings measured with inductively coupled plasma optical emission spectrometry (ICP-OES) are 0.40, 0.40, and 0.37 wt% for AuNC/(C–TiO_2), AuNC@(C–TiO_2), and AuNP/(C–TiO_2), respectively.

Photocatalytic aerobic oxidation of IPA served as a model reaction to evaluate the visible-light (λ = 480–910 nm) photocatalytic performance. Acetone was found to be the main oxidation product in these processes, so it was selected as the comparison parameter for photocatalytic activity. Firstly, C–TiO_2 was subjected to visible-light aerobic oxidation of IPA (**Figure 7**a). As expected, TiO_2-Commercial shows negligible activity under visible-light irradiation. However, 1.8 μmol of acetone was obtained when using C–TiO_2 as the catalyst for 5 h, indicating that a visible-light response is successfully achieved by the incorporation carbon into titania. Taking into account the C–TiO_2 absorption edge at 430 nm, the observed activity is mainly induced by the carbon at the C–TiO_2 surface rather than carbon doped into the inner lattice. Similar phenomena have been demonstrated by several research groups.[9,11] Impressively, after introducing Au NCs to the system (i.e., AuNC/(C–TiO_2)), 5.7 μmol of acetone was obtained following a 5-h reaction time; this is equivalent to 6.3 μmol h^{-1} g^{-1}, which is 3.2 times as much as that obtained over C–TiO_2. In order to eliminate the heating effect, a dark reaction at 40 °C over Janus AuNC/(C–TiO_2) was carried out, and only 0.51 of μmol acetone was obtained. This activity, which is much lower than the photocatalytic activity (i.e., with irradiation), is likely caused by the intrinsic thermocatalytic activity of gold, as also observed elsewhere;[39] that is, the observed visible-light photocatalytic IPA oxidation over Janus AuNC/(C–TiO_2) should be mainly induced by the plasmonic enhancement of the Au NCs. For C–TiO_2, negligible activity was observed in the dark reaction (Figure S8, SI). Reactions over AuNC@(C–TiO_2) and AuNP/

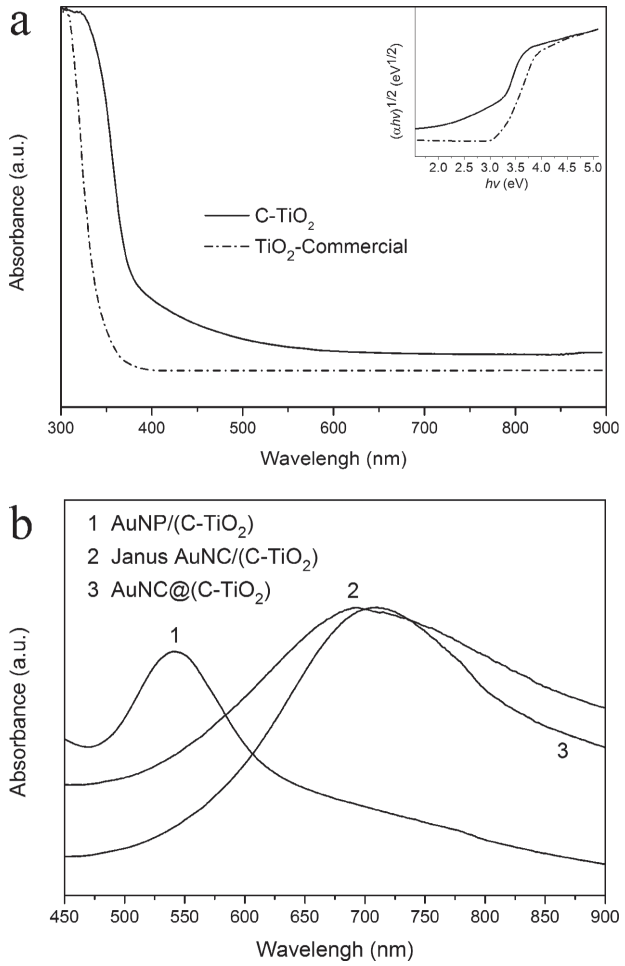

Figure 5. a) UV–vis absorption spectra of C–TiO_2 and TiO_2-Commercial. Inset: Tauc plot. b) UV–vis absorption spectra for the AuNP/(C–TiO_2) system, Janus AuNC/(C–TiO_2) composites, and AuNC@(C–TiO_2) core–shell particles.

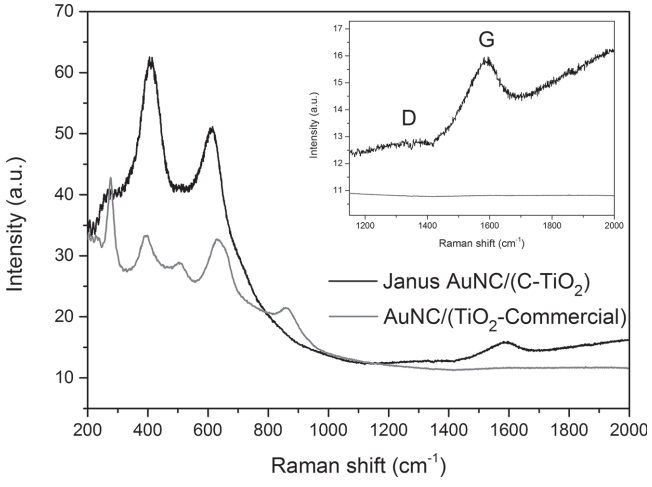

Figure 6. Raman scattering spectra of Janus AuNC/(C–TiO_2) and AuNC/(TiO_2-Commercial). Inset shows the location of the G- and D-bands.

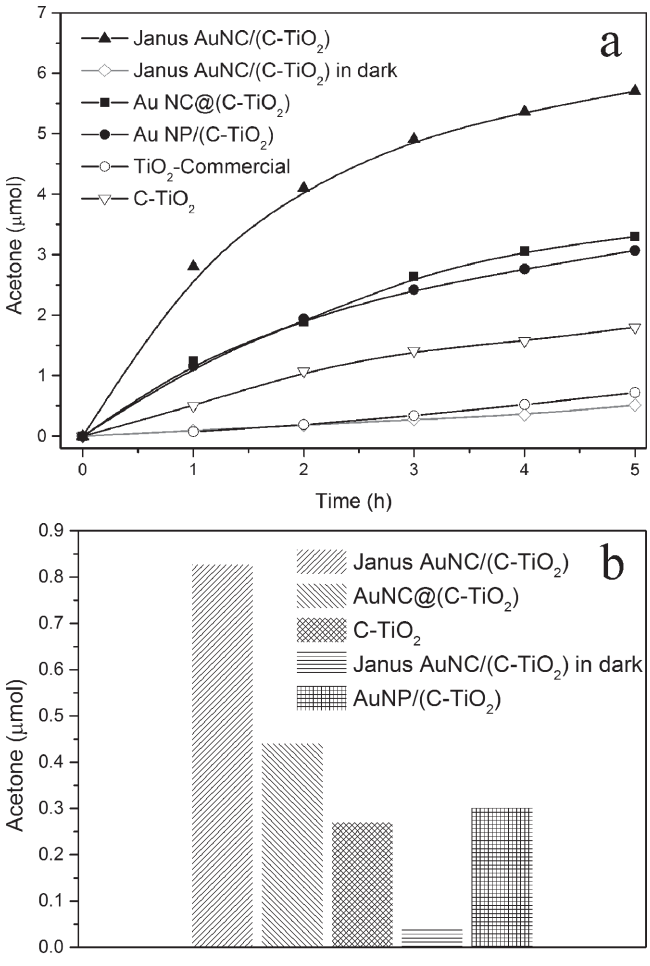

Figure 7. Acetone evolution from a) the photocatalytic oxidation of IPA over various photocatalysts and b) from the analogous reaction carried out under monochromatic light (709 nm) irradiation for 13.5 h.

(C–TiO_2) were also carried out with the purpose of studying the structure and morphology effect. A decrease in photocatalytic oxidation activity was observed when Au NCs were surrounded by a C–TiO_2 shell (AuNC@(C–TiO_2)). The superior activity over Janus AuNC/(C–TiO_2) might be caused by preferential localization of the plasmonic near-fields close to the interface of the Au NC and C–TiO_2 particle, as suggested elsewhere.[24] Interestingly, an inferior activity (3.3 μmol acetone) was also observed over AuNP/(C–TiO_2) although the LSPR of Au NPs are at shorter wavelengths than that of Au NCs; this might be due to the hollow interior and porous walls of the Au NC being manifested as a large number of "hot spots" and due to the inharsh redox potentials required for photocatalytic IPA oxidation.[40]

In hopes of insights into the driving force of the photocatalytic enhancement over the AuNC/(C–TiO_2) composites, IPA photo-oxidation under monochromic light (709 nm) irradiation was first carried out (Figure 7b). The amount of acetone obtained over Janus AuNC/(C–TiO_2) was 0.83 μmol, which is about 3.1 times as much as that obtained over C–TiO_2 (0.27 μmol acetone) under the same reaction conditions. Also, the activity is about 20 times higher than that obtained for the dark reaction (0.04 μmol acetone). Moreover, as expected, the

activity over the AuNP/(C–TiO_2) system was only slightly higher than that of C–TiO_2 because the LSPR absorption of Au NPs is very limited at 709 nm. To further confirm that the observed activities are mainly due to the plasmonic enhancement, we compared the LSPR absorbance spectrum with the photocatalytic enhancement factor ($f_{enhancement}$) plot, where $f_{enhancement}$ was defined as the ratio of the rates for acetone production of Janus AuNC/(C–TiO_2) and C–TiO_2.[41] The spectral profile of $f_{enhancement}$ bears a resemblance to the LSPR absorbance of Janus AuNC/(C–TiO_2) (Figure S9, SI). This result is in accordance with similar conclusions drawn in early works where photocatalytic activity induced by LSPR had also been found at long wavelengths.[18,19,39] The wavelength-dependent performance gives clear evidence that the IPA photo-oxidation over the C–TiO_2 hybrid can be largely enhanced by the plasmons of Au NCs over a broad range of visible light, which largely extends the plasmonic enhancement from about 520 nm for the spherical Au particle to even the near-infrared region.

Photo-electrochemical (PEC) performance over composite materials were carried out with a three-electrode configuration. Linear-sweep voltammetry (LSV) under visible-light (λ > 420 nm) illumination within the potential range of –1.0 to 0.9 V versus Ag/AgCl are available in the SI (Figure S10). Although not obvious as compared with C–TiO_2, the negative shift of onset potential (corresponding to the flatband potential) can also be recognized over Janus AuNC/(C–TiO_2). The photocurrent of the C–TiO_2 film with and without Au NCs irradiated with visible light—i.e., current–time (*I–t*) curves—are shown in **Figure 8**a. The addition of Au NCs results in about a five-fold increase in the photocurrent compared to that of the pure C–TiO_2 film, which means the electron density in the composite is largely enhanced by the presence of Au NCs. It should be pointed out that the photocurrent response even with the Au NC is relatively low—particularly when compared with annealed Au/TiO_2 materials.[42,43] This is likely caused by the weak interaction between the Au NCs and C–TiO_2 due to the presence of carbon and the relatively low Au loading. On the other hand, "hill-like" photo-electroresponses—particularly for Janus AuNC/(C–TiO_2)—suggest a slow photo-electroresponse during and after light irradiation. Generally, introducing carbon materials, such as carbon nanotubes and graphene, into semiconductors will improve the charge-carrier separation, and ultimately make the photocurrent response rise and fall more quickly.[44] In order to clarify the role played by carbon in this study, an oxidative $HClO_4$ treatment developed in our previous work was employed over the Janus AuNC/(C–TiO_2) catalyst in order to remove the carbon.[20] As can be seen from Figure 8b, the "slow photo-electroresponse" phenomenon was obviously restrained. When the C–TiO_2 of the Janus system was replaced with commercial TiO_2, the "hill-like" peaks disappeared. These results indicate that carbon between the Au NC and TiO_2 account for the "slow photo-electroresponse", suggesting that excited electrons can be stored within the carbon sites at the interface of the Au NC and the TiO_2 particle. This enables the carbon to serve as an electron reservoir, which is helpful for plasmonic enhancement when taking into account the ultrafast plasmonic electron transfer from Au to TiO_2.[45]

The stability and integrity of the Janus AuNC/(C–TiO_2) nanocomposite during the aerobic oxidation and the PEC

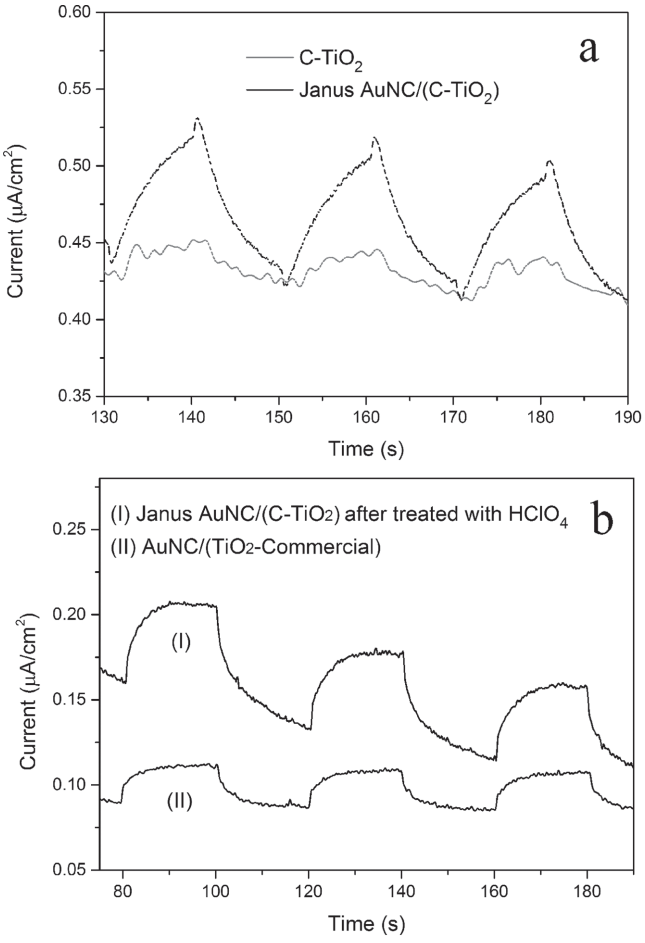

Figure 8. a) Photocurrent of C–TiO_2 with and without Au NCs irradiated with visible light. b) Photocurrent of Janus AuNC/(C–TiO_2) after the $HClO_4$ treatment and of AuNC/(TiO_2-Commercial). Conditions: three-electrode system with working electrode, counter electrode: Pt, and reference electrode: Ag/AgCl; electrolyte: 1 M NaOH; a bias of 0.2 V vs Ag/AgCl; visible light (λ > 420 nm); incident light intensity: 107 mW cm^2.

measurements were studied with TEM and XRD. The composition as well as nanostructure was maintained during IPA photodegradation (Figure S6 and S11a, SI). In the PEC studies, slight aggregation of C–TiO_2 and erosion of the Au NCs can be observed (Figure S11b, SI); these might be caused by the bias applied and basic conditions employed for the investigations.

Physically, LSPR can be described as the resonant photon-induced collective oscillation of valence electrons, while the movement of the electrons result in the corresponding magnetic field, which can serve as an indicator of LSPR states. Electromagnetic simulation of the Janus AuNC/(C–TiO_2) composite was carried out using the RCWA and FDTD methods (**Figure 9**), which are the rigorous coupled-wave analysis and finite-difference time-domain methods, respectively. The electric-field plane-wave propagating along the *Z* axis oscillates in the *XZ* plane, which is parallel to the cross-section of the Janus AuNC/(C–TiO_2). The simulated absorption of Janus AuNC/(C–TiO_2) is similar to its experimental UV–vis absorption (Figure 9a), indicating the simulation model works well. The cross-sectional contour-plot field distribution in the *XY*

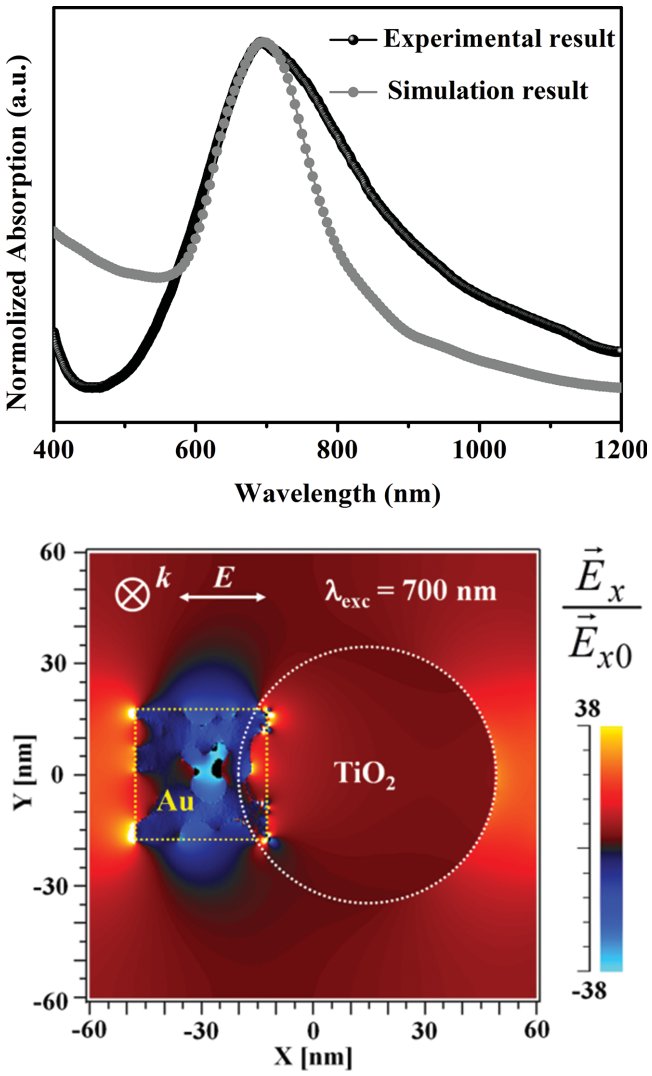

Figure 9. Up: Absorption spectra of Janus AuNC/(C–TiO_2) from simulation and experiment. Down: Electromagnetic field distribution and enhancement simulated with the FDTD method. Simulated electric field distribution—E_x normalized to the incident field—E_{x0} around the Janus AuNC/(C-TiO2). The excitation wavelength, λ_{exc}, was 700 nm; *k* indicates the wave-vector; the color scale bar shows the electric field enhancement, E_x/E_{x0}, with the negative and positive electric field amplitudes.

plane is shown in Figure 9b. As can be seen, the electric field enhancement at the interface of the Au NC and C–TiO_2 in the Janus system reaches 38 times that of the incident electromagnetic field. Correspondingly, the field intensity ($|E|^2$) is about 1400 times higher than that of the incident one, indicating a dramatic amplification of the plasmon–photon coupling effect at the AuNC/(C–TiO_2) interface. These "hot spots" indicate the generation of a high density of energetic electrons at the interface via resonant excitation of the Au NC plasmon.

The carbon within C–TiO_2 prepared via solvothermal techniques has been found to show graphite-like properties, while its electron coupling with TiO_2 accounts for the visible-light activity of C–TiO_2.[9] Janus AuNC/(C–TiO_2) and C–TiO_2 were evaluated using EPR at 4.2 K (Figure S12, SI), both before and after visible-light irradiation. A broad signal with a *g* value of 2.0039 ± 0.0003 was observed for C–TiO_2 in the dark. This peak arises from the paramagnetic center of the carbon—more specifically, a π-type and/or σ-type center.[46,47] The intensity of this peak decreased after introducing the Au NCs, which is likely caused by the delocalization of the electrons.[46] Visible-light irradiation of C–TiO_2 resulted in the peak slightly increasing in intensity, indicating that there was no obvious change in the electron distributions at the carbon centers. This result suggests that electrons excited from C–TiO_2 under visible-light irradiation are limited, which is consistent with its IPA-photodegradation performance. In contrast, a very strong carbon paramagnetic signal was observed for Janus AuNC/(C–TiO_2) after visible-light irradiation, indicating intense electron accumulation at the carbon. Taking into account the relatively low EPR response over C–TiO_2 under visible-light irradiation and Janus AuNC/(C–TiO_2) in dark, these electrons probably come from either the Au NCs or the C–TiO_2 induced by the electromagnetic field of the Au NCs. Because LSPR-induced electromagnetic field decays exponentially with distance while Au NCs are separated from C-TiO_2 by carbon derivative,[48] these electrons that are accumulated at the carbon under irradiation are most likely from the energetic plasmonic electrons that had been excited in the Au NCs. This assumption is supported by the simulation results, which indicate that the plasmon–photon coupling is dramatically amplified at AuNC/(C–TiO_2) interface, indicating the generation of a high density of energetic electrons at the interface via resonant excitation of the Au NC plasmon. Subsequently, the electrons transfer to the conduction band of TiO_2, where they can activate O_2 to intermediates (O_2^- and/or H_2O_2) that can be involved in further oxidation.[49–51] Although different from the general electronic interaction in metal and semiconductor composites, e.g., the Schottky junction, electron transfer from coinage metals to semiconductors has been proven to play an important role in the photosensitization and photocatalytic enhancement under visible-light irradiation.[34,52]

3. Conclusion

In summary, we have demonstrated a novel and facile method for preparation of non-centrosymmetric Janus AuNC/(C–TiO_2), which is capable of plasmonic visible-light harvesting over a broad range. Prominent plasmonic enhancement is achieved with Janus AuNC/(C–TiO_2) for both the photocatalytic aerobic oxidation of *iso*-propanol and photo-electrocatalytic evaluations. Electromagnetic field simulations and electron paramagnetic resonance results indicate plasmon–photon coupling is largely amplified at the interface between the Au NC and C–TiO_2 of Janus AuNC/(C–TiO_2), leading to the enhanced generation of energetic hot electrons for photocatalysis. The strategy reported here for preparing an asymmetric Janus nanostructure and for introducing gold nanocages might open an avenue for developing efficient visible-light-sensitive photocatalysts.

4. Experimental Section

Hybrid C–TiO_2 Nanocrystals: C–TiO_2 nanocrystals were prepared using conventional hydrothemal synthesis without any external carbon precursors.[13] Generally, NH_4HCO_3 (3 g), cyclohexane (15 mL), oleic

acid (45 mL), and triethylamine (15 mL) were mixed together at room temperature, followed by the dropwise addition of 3 mL of titanium tetra-*iso*-propoxide ($Ti(OPr)_4$) and stirring for 2 min. The solution was then transferred to an autoclave at 150 °C for 24 h. After thoroughly washing with acetone, C–TiO_2 nanocrystals were redispersed in cyclohexane, and a brown sol was obtained.

Preparation of Au NCs and Au NPs: The Ag nanocube template with an edge length of about 35 nm was first synthesized via a polyol method as described elsewhere.[53] In a typical synthesis, ethylene glycol (EG, 70 mL) was heated at 150 °C while stirring for 1 h. Then, a solution of PVP (molecular weight (MW) 55 kDa, Aldrich, 0.85 g) in EG was added. After 5 min, $Na_2S{\cdot}9H_2O$ (0.4 mL, 3 mmol/L, Aldrich) and $AgNO_3$ (6 mL, 60 mg/mL), each dissolved in EG, were sequentially injected. After about 10 min, the solution changed to an opalescent ruddy-brown and concurrently became opaque. Au NCs were prepared with a galvanic replacement reaction. In a typical synthesis, a fixed amount (10 mL) of the as-synthesized silver nanocubes was washed twice with distilled water. After being collected by centrifugation, the Ag nanocubes were redispersed in 100 mL of water and then heated to boil for 10 min. An aqueous solution of $HAuCl_4$ (0.5 mmol/L) was added to the flask through a syringe pump under magnetic stirring. The solution was heated for another 10 min until the color of the system was stable. AgCl was dissolved by adding NaCl, and the Au NCs were collected following centrifugation. Au NPs were prepared with the Frens' method.[54] In a typical process, an aliquot of an aqueous $HAuCl_4$ solution (100 mL, 0.25 mM) was heated to boiling, and trisodium citrate (10 mL, 1%) was added. After ≈10 min, the solution was set aside to cool down to room temperature, and then washed with ultrapure water.

Preparation of Janus AuNC/(C–TiO_2), AuNC@(C–TiO_2), AuNP/(C–TiO_2), and Au NC/TiO_2-Commerical: Asymmetric Janus AuNC/(C–TiO_2) and AuNC@(C–TiO_2) composite nanostructures were prepared by a novel method developed in this work based on a bottom-up assembly method reported elsewhere.[55] In a general preparation, as-prepared Au NCs dispersed in water (6 mL), C–TiO_2 nanocrystals dispersed in cyclohexane (5 mL), and SDS (0.112 g) were added to deionized water (18 mL). A microemulsion formed with stirring, after which ethanol (0.5 or 1.0 mL) was added. An oil-in-water emulsion was formed through vigorous stirring. Then, cyclohexane was removed by heating at 70 °C with constant stirring in the presence of an Ar flow for 4 h, leading to the assembly of the composite comprising a Au NC and a C–TiO_2 particle After the reaction was cooled to room temperature, products were collected, washed with water, and vacuum-dried at 80 °C overnight. A composite system, in which Au NPs decorate a C–TiO_2 nanocrystal (AuNP/(C–TiO_2)), and the hybrid C–TiO_2 were prepared by similar methods and employed as references. Au NC/TiO_2-Commerical prepared with impregnation method was employed for comparision in Raman scattering measurement.

Characterization: Both UV–vis absorption and UV–vis diffuse reflectance spectra were recorded with a Shimadzu UV-2600, while an integrating sphere was used in diffusion reflectance adsorption analysis. Samples for TEM analysis were prepared by drying a drop of nanocrystal dispersion in water on amorphous carbon–coated copper grids. TEM characterization was performed with a JEOL 2100F operated at 200 kV. XPS experiments were performed in a Theta probe (Thermo Fisher) using monochromated Al Kα X-rays. XRD patterns of the products were recorded on an X-Pert diffractometer equipped with graphite-monochromatized Cu–Kα radiation. The Brunauer–Emmett–Teller (BET) surface areas were measured via nitrogen physisorption (Gemini-2360; Micromeretics Corp., USA). EPR characterizations were carried out with JEOL JES-FA-200 at 4.2 K achieved using liquid helium. The gold loadings were measuered with ICP-OES, Nippon Jarrell-Ash Co. data TTG/DTA data were obtained on a Shimadzu DTG-60H DTA-TG apparatus under air flow. Raman spectra were obtained on an NRS-1000 Laser Raman Spectrophotometer (Jasco Inc., Japan) with a laser source at 532 nm.

*Photo*catalytic *and Photo-electrocatalytic Performance*: Typically, 0.18 g of the AuNC/(C–TiO_2) catalyst was spread uniformly in a quartz vessel with an irradiation area of 9.0 cm^2. The CO_2-containing natural air sealed in the vessel was replaced by ≈1 atm of artificial pure air (O_2/N_2 = 1/9). Then, a certain amount of gaseous *iso*-propanol was injected into the vessel. Prior to light irradiation, the vessel was kept in the dark for 1.5 h until an adsorption–desorption equilibrium was finally established. Visible light between 480 and 910 nm was obtained by using Y50+R900+water filters. The light source was a 300-W Xe lamp. Dark reactions carried out at 40 °C were used to evaluate the thermal effect. In order to further confirm that the photocatalytic oxidation of IPA can be induced by the plasma of Au NCs, photocatalytic reactions under monochromatic light at 709 nm, which is close to the characteristic plasmon adsorption position, were also carried out. Photocatalytic enhancement factor ($f_{enhancement}$) at various wavelengths was measured by inserting a water filter and various band-pass filters (Optical Coatings Japan) in front of the reaction cell to obtain the desired incident wavelength. For each wavelength region, the irradiation lasted for 4 h. The products were analyzed with a gas chromatograph system (GC-2014, Shimadzu, Japan) with a flame ionization detector (FID). AuNC/(C–TiO_2) as well as the C–TiO_2 electrode was prepared by a spin-coating method. For comparison, the Janus AuNC/(C–TiO_2) composite was treated with oxidative $HClO_4$ to remove carbon as developed in our previous work.[20] For additional comparisons, AuNC/(TiO_2-Commercial) was prepared using an immigration method with commercial TiO_2 (Wako Pure Chemical Industries, Ltd.). Electrodes comprising these two materials were also prepared by spin-coating. Photo-electrochemical properties were measured in a three-electrode configuration. The working electrode was a AuNC/(C–TiO_2) or C–TiO_2 electrode; the counter electrode, Pt; the reference electrode, Ag/AgCl (saturated KCl, RE-1C; BAS Inc.); and the electrolyte, 1 M NaOH. A 500-W Xe lamp (Optical ModuleX; Ushio Inc.) was used as the solar light source. A Y44 filter was used to get visible light ($\lambda > 420$ nm), and the incident light intensity at 420–800 nm was measured to be 107 mW cm^2 using a spectroradiometer (USR-40; Ushio Inc.). LSV was performed with a voltage scan speed of 0.05 V s^{-1}. For *I–t* measurements, a bias of 0.2 V vs Ag/AgCl was used and the light was chopped manually at regular intervals.

Theoretical Simulations: The absorption spectra of Au NCs on TiO_2 were calculated by using a numerical solver based on the RCWA method (Diffractmod, Rsoft Design). The electric field distribution in the vicinity of a Janus Au–TiO_2 structure was calculated by another numerical solver based on the FDTD method (Fullwave package, Rsoft). The dielectric functions of Au and anatase TiO_2 were taken from literature.[56,57]

Supporting Information

Supporting Information is available from the Wiley Online Library or from the author.

Acknowledgements

This work received financial support from the World Premier International Research Center Initiative (WPI Initiative) on Materials Nanoarchitectonics (MANA) and the National Basic Research Program of China (973 Program, 2014CB239301).

Received: June 24, 2014
Revised: September 14, 2014
Published online: October 14, 2014

[1] H. Tong, S. Ouyang, Y. Bi, N. Umezawa, M. Oshikiri, J. Ye, *Adv. Mater.* **2012**, *24*, 229.
[2] D. F. Wang, T. Kako, J. H. Ye, *J. Am. Chem. Soc.* **2008**, *130*, 2724.
[3] M. R. Hoffmann, S. T. Martin, W. Choi, D. W. Bahnemann, *Chem. Rev.* **1995**, *95*, 69.
[4] A. Fujishima, K. Honda, *Nature* **1972**, *238*, 37.
[5] X. Chen, S. S. Mao, *Chem. Rev.* **2007**, *107*, 2891.

[6] W. Choi, A. Termin, M. R. Hoffmann, *J. Phys. Chem.* **1994**, *98*, 13669.
[7] R. Asahi, T. Morikawa, T. Ohwaki, K. Aoki, Y. Taga, *Science* **2001**, *293*, 269.
[8] S. U. M. Khan, M. Al-Shahry, W. B. Ingler, *Science* **2002**, *297*, 2243.
[9] L.-W. Zhang, H.-B. Fu, Y.-F. Zhu, *Adv. Funct. Mater.* **2008**, *18*, 2180.
[10] Y. Zhang, C. Pan, *J. Mater. Sci.* **2010**, *46*, 2622.
[11] H. Zhang, X. Lv, Y. Li, Y. Wang, J. Li, *ACS Nano* **2010**, *4*, 380.
[12] J. Yu, G. Dai, Q. Xiang, M. Jaroniec, *J. Mater. Chem.* **2011**, *21*, 1049.
[13] Y. Park, W. Kim, H. Park, T. Tachikawa, T. Majima, W. Choi, *Appl. Catal. B* **2009**, *91*, 355.
[14] S. Linic, P. Christopher, D. B. Ingram, *Nat. Mater.* **2011**, *10*, 911.
[15] Y. Tachibana, L. Vayssieres, J. R. Durrant, *Nat. Photonics* **2012**, *6*, 511.
[16] P. Christopher, D. B. Ingram, S. Linic, *J. Phys. Chem. C* **2010**, *114*, 9173.
[17] Y. Nishijima, K. Ueno, Y. Kotake, K. Murakoshi, H. Inoue, H. Misawa, *J. Phys. Chem. Lett.* **2012**, *3*, 1248.
[18] S. Mubeen, J. Lee, N. Singh, S. Kramer, G. D. Stucky, M. Moskovits, *Nat. Nanotechnol.* **2013**, *8*, 247.
[19] Z. Zheng, T. Tachikawa, T. Majima, *J. Am. Chem. Soc.* **2014**, *136*, 6870.
[20] L. Liu, S. Ouyang, J. Ye, *Angew. Chem. Int. Ed.* **2013**, *52*, 6689.
[21] W. B. Hou, W. H. Hung, P. Pavaskar, A. Goeppert, M. Aykol, S. B. Cronin, *ACS Catal.* **2011**, *1*, 929.
[22] J. Z. Zhang, C. Noguez, *Plasmonics* **2008**, *3*, 127.
[23] J. Chen, B. Wiley, Z. Y. Li, D. Campbell, F. Saeki, H. Cang, L. Au, J. Lee, X. Li, Y. Xia, *Adv. Mater.* **2005**, *17*, 2255.
[24] Z. W. Seh, S. Liu, M. Low, S. Y. Zhang, Z. Liu, A. Mlayah, M. Y. Han, *Adv. Mater.* **2012**, *24*, 2310.
[25] Q. Zhang, D. Q. Lima, I. Lee, F. Zaera, M. F. Chi, Y. D. Yin, *Angew. Chem. Int. Ed.* **2011**, *50*, 7088.
[26] P. Ghenuche, S. Cherukulappurath, T. H. Taminiau, N. F. van Hulst, R. Quidant, *Phys. Rev. Lett.* **2008**, 101.
[27] J. B. Lassiter, J. Aizpurua, L. I. Hernandez, D. W. Brandl, I. Romero, S. Lal, J. H. Hafner, P. Nordlander, N. J. Halas, *Nano Lett.* **2008**, *8*, 1212.
[28] S. Pradhan, D. Ghosh, S. W. Chen, *ACS Appl. Mater. Interfaces* **2009**, *1*, 2060.
[29] Z. W. Seh, S. Liu, S. Y. Zhang, M. S. Bharathi, H. Ramanarayan, M. Low, K. W. Shah, Y. W. Zhang, M. Y. Han, *Angew. Chem. Int. Ed.* **2011**, *50*, 10140.
[30] B. K. Paul, S. P. Moulik, *J. Dispersion Sci. Technol.* **1997**, *18*, 301.
[31] P. G. De Gennes, C. Taupin, *J. Phys. Chem.* **1982**, *86*, 2294.
[32] A. M. Cazabat, D. Langevin, J. Meunier, A. Pouchelon, *Adv. Colloid Interface Sci.* **1982**, *16*, 175.
[33] G. Wu, T. Nishikawa, B. Ohtani, A. Chen, *Chem. Mater.* **2007**, *19*, 4530.
[34] L. Liu, P. Li, A. Boonchun, S. Ouyang, N. Umezawa, J. Ye, R. Kodiyath, T. Tanabe, R. V. Gubbala, S. Ueda, H. Abe, *J. Mater. Chem. A* **2014**, *2*, 9875.
[35] S. Link, M. A. El-Sayed, *Annu. Rev. Phys. Chem.* **2003**, *54*, 331.
[36] Q. J. Xiang, J. G. Yu, B. Cheng, H. C. Ong, *Chem. Asian J.* **2010**, *5*, 1466.
[37] T. Wang, J. Tang, X. Fan, J. Zhou, H. Xue, H. Guo, J. He, *Nanoscale* **2014**, *6*, 5359.
[38] W. Ren, Z. Ai, F. Jia, L. Zhang, X. Fan, Z. Zou, *Appl. Catal. B* **2007**, *69*, 138.
[39] E. Kowalska, O. O. P. Mahaney, R. Abe, B. Ohtani, *Phys. Chem. Chem. Phys.* **2010**, *12*, 2344.
[40] M. A. Mahmoud, M. A. El-Sayed, *J. Am. Chem. Soc.* **2010**, *132*, 12704.
[41] T. Torimoto, H. Horibe, T. Kameyama, K.-I. Okazaki, S. Ikeda, M. Matsumura, A. Ishikawa, H. Ishihara, *J. Phys. Chem. Lett.* **2011**, *2*, 2057.
[42] Z. Zhang, L. Zhang, M. N. Hedhili, H. Zhang, P. Wang, *Nano Lett.* **2013**, *13*, 14.
[43] Z. W. Liu, W. B. Hou, P. Pavaskar, M. Aykol, S. B. Cronin, *Nano Lett.* **2011**, *11*, 1111.
[44] D. Wang, J. K. Baral, H. Zhao, B. A. Gonfa, V.-V. Truong, M. A. El Khakani, R. Izquierdo, D. Ma, *Adv. Funct. Mater.* **2011**, *21*, 4010.
[45] A. Furube, L. Du, K. Hara, R. Katoh, M. Tachiya, *J. Am. Chem. Soc.* **2007**, *129*, 14852.
[46] R. C. Barklie, *Diamond Relat. Mater.* **2003**, *12*, 1427.
[47] A. B. Bourlinos, E. P. Giannelis, Y. Sanakis, A. Bakandritsos, M. Karakassides, M. Gjoka, D. Petridis, *Carbon* **2006**, *44*, 1906.
[48] E. A. Coronado, E. R. Encina, F. D. Stefani, *Nanoscale* **2011**, *3*, 4042.
[49] E. Kowalska, R. Abe, B. Ohtani, *Chem. Commun.* **2009**, 241.
[50] Y. Sugano, Y. Shiraishi, D. Tsukamoto, S. Ichikawa, S. Tanaka, T. Hirai, *Angew. Chem. Int. Ed.* **2013**, *52*, 5295.
[51] H. M. Chen, C. K. Chen, C.-J. Chen, L.-C. Cheng, P. C. Wu, B. H. Cheng, Y. Z. Ho, M. L. Tseng, Y.-Y. Hsu, T.-S. Chan, J.-F. Lee, R.-S. Liu, D. P. Tsai, *ACS Nano* **2012**, *6*, 7362.
[52] Y. Tian, T. Tatsuma, *Chem. Commun.* **2004**, 1810.
[53] A. R. Siekkinen, J. M. McLellan, J. Chen, Y. Xia, *Chem. Phys. Lett.* **2006**, *432*, 491.
[54] G. Frens, *Nat. Phys. Sci.* **1973**, *241*, 20.
[55] F. Bai, D. Wang, Z. Huo, W. Chen, L. Liu, X. Liang, C. Chen, X. Wang, Q. Peng, Y. Li, *Angew. Chem. Int. Ed.* **2007**, *46*, 6650.
[56] E. D. Palik, *Handbook of Optical Constants of Solids*, Academic Press, San Diego, CA **1998**.
[57] N. Hosaka, T. Sekiya, C. Satoko, S. Kurita, *J. Phys. Soc. Jpn.* **1997**, *66*, 877.